



City Research Online

City, University of London Institutional Repository

Citation: Evangelou, S. A., Limebeer, D. J. N. & Tomas-Rodriguez, M. (2013). Suppression of Burst Oscillations in Racing Motorcycles. Paper presented at the 49th IEEE Conference on Decision and Control, 15-12-2010 - 17-12-2010, Atlanta, USA. doi: 10.1115/1.4006491

This is the accepted version of the paper.

This version of the publication may differ from the final published version.

Permanent repository link: <https://openaccess.city.ac.uk/id/eprint/12551/>

Link to published version: <https://doi.org/10.1115/1.4006491>

Copyright: City Research Online aims to make research outputs of City, University of London available to a wider audience. Copyright and Moral Rights remain with the author(s) and/or copyright holders. URLs from City Research Online may be freely distributed and linked to.

Reuse: Copies of full items can be used for personal research or study, educational, or not-for-profit purposes without prior permission or charge. Provided that the authors, title and full bibliographic details are credited, a hyperlink and/or URL is given for the original metadata page and the content is not changed in any way.

City Research Online:

<http://openaccess.city.ac.uk/>

publications@city.ac.uk

Suppression of Burst Oscillations in Racing Motorcycles

Simos A. Evangelou, David J. N. Limebeer and Maria Tomas-Rodriguez

Abstract—Burst oscillations occurring at high speed and under firm acceleration are suppressed with a mechanical steering compensator. Burst instabilities in the subject racing motorcycle are the result of interactions between the wobble and weave modes under high-speed cornering and firm-acceleration conditions. Under accelerating conditions the wobble-mode frequency decreases, while the weave mode frequency increases so that destabilizing interactions occur. The design analysis is based on a time-separation principle, which assumes that bursting occurs on time scales over which speed variations can be neglected. Therefore, under braking and acceleration conditions linear time-invariant models corresponding to constant-speed operation can be utilized in the design process. The inertial influences of braking and acceleration are modelled using d’Alembert-type forces that are applied at the mass centres of each of the model’s constituent bodies. The resulting steering compensator is a simple mechanical network that comprises a conventional steering damper in series with a linear spring. This network is a mechanical lag compensator.

I. INTRODUCTION

High-speed steering oscillations are potentially dangerous for racing motorcyclists. In the case of the motorcycle studied here, measurement data reveals the presence of steering oscillations under high-speed acceleration conditions. Figure 1 (a) shows the measured speed, acceleration, roll angle and damper stroke velocity of the subject motorcycle on a particular section of race track. Since the frequency of these oscillations is of the order 28 rad/s, weave-type behaviour is suspected. A short-period Fourier transform of the damper velocity signal is displayed in Figure 1 (b). This plot confirms that a steering oscillation of approximately 28 rad/s persists for approximately 4 s. Our purpose is to investigate the underlying causes of the bursting phenomenon illustrated in Figure 1 (a) using a high-fidelity computer model, and then find a means of damping these oscillations with a mechanical steering compensator. Similar techniques have already been used to improve the constant-speed dynamic performance of a road-going sports machine [1]. A key difference between the study in [1] and this one is the need to deal with variable speeds. The predominant lateral oscillations in two-wheeled vehicles are ‘wobble’ and ‘weave’. In straight running the weave mode is well damped at moderate speeds, but becomes less so at elevated speeds. The natural frequency rises from zero at walking speeds to somewhere in the range 2-4Hz,

This work was supported by the UK Engineering and Physical Sciences Research Council. Simos A. Evangelou (s.evangelou@imperial.ac.uk) has appointments with the Departments of Electrical and Electronic, and Mechanical Engineering at Imperial College London. David J. N. Limebeer (david.limebeer@eng.ox.ac.uk) is Professor of Control Engineering, Department of Engineering Science, University of Oxford. Maria Tomas-Rodriguez (Maria.Tomas-Rodriguez.1@city.ac.uk) is with the Mathematics and Engineering Department at City University London.

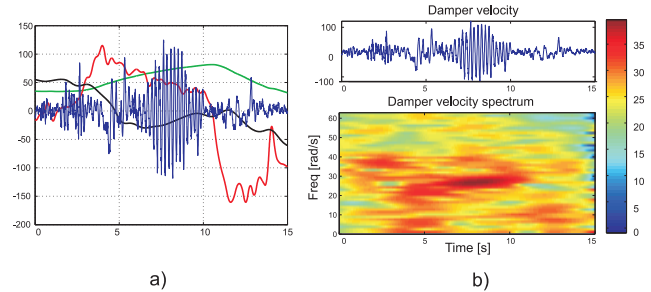


Fig. 1. (a) Measured test data for the subject racing motorcycle. The green trace shows the speed in m/s, the red trace shows the acceleration ($\times 10 \text{ m/s}^2$), the black trace is the motorcycle’s roll angle (degs) and the blue trace represents the damper velocity in mm/s. Oscillatory steering bursting is visible at 8 s and corresponds to a speed of approximately 70 m/s under approximately 5 m/s^2 of acceleration. The frequency of the bursting is 28 rad/s and corresponds to a weave-type oscillation. (b) Short-period Fourier Transform of the damper stroke rate signal illustrated in (a). A weave-like burst oscillation occurs at approximately 8 s and persists for approximately 4 s; the signal amplitude is given in decibels.

depending on the mass and size of the machine; lower frequencies corresponding to heavier motorcycles. Computer studies indicate that the torsional stiffness of the motorcycle frame at the steering head will determine if the machine is prone to wobbling at medium or high speeds. In the case of compliant frames of the type associated with older touring motorcycles wobble oscillations tend to occur at modest speeds. In the case of stiff-framed sports machines, wobble-mode instabilities become a high-speed phenomenon [2], [3]. The frequency of the wobble mode is relatively insensitive to speed, and is governed primarily by the mechanical trail, the front tire cornering stiffness and the front frame steer inertia. The frequency of the wobble mode is normally in the range 6-9Hz. Stiff framed machines, being prone to wobbling at high speed, often depend on a steering damper for wobble-mode damping. While having a stabilizing influence on the wobble mode, a steering damper will usually destabilize the weave mode at high-speed and a compromise between high and low damper values has to be found. Acceleration is an operating regime of central importance to the present study, since it is under these conditions that the bursting oscillations illustrated in Figure 1 (a) occur. Relatively little has been written on the dynamics of two-wheeled road vehicles under acceleration and braking. Reference [4] presents a study of the accelerating straight-running bicycle, which extends the fixed-speed study presented in [5]. Some early work on the dynamics of accelerating motorcycles can be found in [6]. This study makes use of a hand-derived model confined to straight-running situations, but the equations

presented contain errors. In a later study the dynamics of the straight-running accelerating motorcycle were revisited [7], where a practical machine model is used that includes a suspension system and realistic tire representations. It was concluded that the motorcycle's wobble mode is noticeably destabilized when the machine descends an incline, or brakes on a level surface. Conversely, the damping of the wobble mode is increased when the machine ascends an incline, or accelerates on a level surface. Except at very low speeds, inclines and acceleration appear to have little effect on the frequency or damping of the weave mode.

The remainder of the paper is structured as follows: Section II describes a high-fidelity model of the subject racing motorcycle. Section III describes the control-theoretic analysis framework used for the design of the steering compensation system. The effect of acceleration and braking on the subject motorcycle is studied in Section IV. Predicted bursting phenomena under firm acceleration are presented in Section IV-A. Analysis of the accelerating machine using constant-speed models is introduced in Section IV-B. The steering compensator design problem and outcomes are presented in Section V. A comprehensive set of results is presented in Section VI with the conclusions in Section VII.

II. MOTORCYCLE MODEL

The model of the subject motorcycle used here is an evolution of prior computer models [8], [9], [10], [11], [12], [13]. This model is based on the following kinematically interconnected rigid bodies: the handlebars, upper and lower front forks separated by a telescopic suspension, the front wheel, the main frame comprising the engine, chassis and rider, the swinging arm, the rear wheel and the engine sprocket that rotates about a transverse axis. It involves three translational and three rotational freedoms of the main frame, a steering freedom associated with the rotation of the front frame relative to the main frame and spinning freedoms of the road wheels. The mathematical model employed here also accommodates front and rear suspension freedoms, frame twisting, aerodynamic forces and moments. The rider is rigidly attached to the main frame. The road tires are treated as wide, flexible in compression, and care is taken to track dynamically the migration of both ground-contact points as the machine rolls, pitches and steers. Both contact points, which are taken as the points closest to the road surface, move laterally over the tires surface; these points represent the center of the road-tire contact patch. The front tire ground contact point will also move circumferentially under combined rolling and steering. The tire forces and moments are generated from the normal load, the tires camber angle relative to the road and the combined slip using modified Magic Formula models [14], which describe the tire behaviour on smooth roads (road obstacle wavelengths longer than the tire radius), and up to frequencies of approximately 8 Hz [15]. This model is applicable to motorcycle tires operating at roll angles of up to 60°. The lateral compliance of the tires' carcass is modelled using linear time-varying stretched-string type tire models.

Relaxation effects for the longitudinal tyre compliance are similarly described. In combination, the relaxation effects have a lagging influence on the generation of the tire forces and moments. The suspension units are modelled as a parallel combination of a nonlinear damper and a nonlinear spring with limit stops. Aerodynamic drag/ lift forces and pitching moment are proportional to the square of the machine's forward speed. The model of the chain system requires one to track dynamically the upper and lower tangent points on the gearbox and rear-wheel sprockets [13]. These points can be described as functions of the swing arm angle. The chain itself is treated as a parallel spring damper combination, and the chain tension can be found with the aid of a chain deflection calculation that converts the chain deflection into a force. In order to maintain steady-state operating conditions, and/or prescribed operating trajectories, the machine simulation has been fitted with a number of simple control systems, which in some sense mimic the rider's control behaviour. These systems control the throttle, the braking and braking distribution between the front and rear wheels, and the vehicle's steering. We refer the reader to [16] for a more detailed description of the suspension system, aerodynamic forces and the tires' force and moments acting on motorcycle model under study.

III. ANALYSIS FRAMEWORK

The steering compensation system will be designed and analysed in the generalized regulator framework popularized by the robust control community [17]. In Figure 2 (a), the exogenous vertical-displacement road-forcing disturbances are represented by the signal $d(s)$, the steering angle is $\delta(s)$ and the steering-compensator-induced torque is given by $t(s)$. In the case of a steering damper, $k(s)$ becomes a constant gain feedback controller k . The 'generalized plant', $P(s)$ is a linear time-invariant model of the subject motorcycle derived from a small-perturbation analysis around an arbitrary trim condition. While Figure 2 (a) shows a frequency-domain model of the linearized system, a setup of this type is equally applicable to nonlinear time-domain studies. If $P(s)$ is partitioned as:

$$P(s) = \begin{bmatrix} p_{11}(s) & p_{12}(s) \\ p_{21}(s) & p_{22}(s) \end{bmatrix},$$

then the generalized regulator configuration in this case is defined by

$$\begin{bmatrix} \delta(s) \\ s\delta(s) \end{bmatrix} = \begin{bmatrix} p_{11}(s) & p_{12}(s) \\ sp_{11}(s) & sp_{12}(s) \end{bmatrix} \begin{bmatrix} d(s) \\ t(s) \end{bmatrix},$$

and $t(s) = k(s)s\delta(s)$, which gives $\delta(s) = (I - sp_{12}(s)k(s))^{-1}p_{11}(s)d(s)$. Repeated reference will be made to the Nyquist criterion of the open-loop system $sk(s)p_{12}(s)$, in which $p_{12}(s)$ maps the steering torque $t(s)$ into the steering angle $\delta(s)$. Figure 2(b) shows straight-running root-loci for the subject motorcycle under open- and closed-loop conditions as a function of the machine speed. The open-loop machine characteristics are shown in the + (red) plot, while those corresponding to the subject

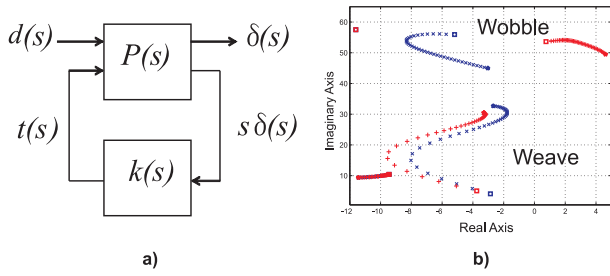


Fig. 2. a) $P(s)$ is a linearized motorcycle model, while $k(s)$ is the steering compensator. ‘ s ’ is the Laplace transform variable. b) Constant-speed straight-running root-loci for the subject motorcycle showing the influence of the steering damper — speed is the swept parameter. The top speed is marked with a star, while the lowest speed is marked with a square symbol.

motorcycle fitted with a steering damper are given by the \times (blue) plot. The speed is varied from 10 m/s to 90 m/s in steps of 2 m/s. As can be seen from this plot the open-loop machine has an unstable wobble mode and a well damped weave mode. Under feedback control, with a steering damper ($k(s) = k$ a constant), the wobble mode is stabilized, but at the expense of a reduction in the weave mode damping. In this work we design a steering compensator $k(s)$, which provides good damping characteristics under constant-speed and accelerating and braking conditions.

IV. ACCELERATION INFLUENCES

A. Simulated Bursting

The study of the influence of acceleration on the dynamics of the subject motorcycle begins by seeking to replicate in the simulation model the measured bursting behaviour illustrated in Figure 1. Bursting is a phenomenon associated with variable speed conditions. Figure 3(a) shows the output from the simulation model of the subject motorcycle under variable speed straight-running conditions. In this simulation the speed reference is $v = v_0 + A \sin(0.2t)$, in which $v_0 = 70$ m/s and $A = 25$ m/s. The machine speed therefore varies sinusoidally between 45 and 95 m/s, while the machine’s acceleration varies between ± 5 m/s². A low-amplitude steering torque disturbance, which represents road disturbances, is introduced into the simulation. The discontinuities in the acceleration signal derive from ‘snap’ in the chain drive as it switches between driving and braking. Under accelerating conditions burst oscillation of amplitude almost 2 rad/s can be observed in the steering angular rate signal — this oscillation is also visible in the machine’s forward acceleration signal. The disturbance appears to begin soon after the motorcycle reaches the peak acceleration of 5 m/s². The spectral content of the steering velocity signal is shown in Figure 3(b). The data between 10 s and 20 s in Figure 3(a) was extracted for further analysis. The bursting frequency increases from approximately 33 rad/s to approximately 38 rad/s in sympathy with increases in the machine speed. Referring to Figure 2 (b), it is noted that this range of frequencies indicates that the burst oscillations correspond to the machine’s weave mode.

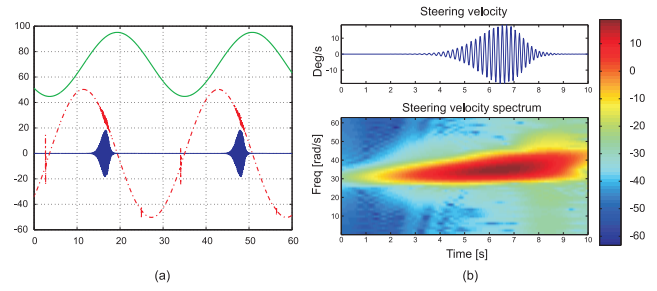


Fig. 3. a) Simulated weave-mode burst oscillations in the subject motorcycle under straight-running conditions. The speed is shown as the solid (green) line, $10 \times$ the acceleration is shown as the dot-dashed (red) line, while $10 \times$ the steering velocity is shown as the solid (blue) bursting characteristic (in rad/s). (b) Short-Period Fourier Transform of the steering velocity signal given in (a). Data between 10 s and 20 s was extracted for analysis - bursting is apparent between 14 s and 18 s (a). The bursting frequency increases from approximately 33 rad/s to approximately 38 rad/s in sympathy with the speed increase on this time interval.

B. Acceleration Analysis

An analysis of the influence of acceleration on the machine stability, which is based on prior bicycle work, is now introduced. By way of background, we remind the reader that a detailed first-principles study of the dynamics of the constant-speed straight-running bicycle can be found in the survey papers [5], [18], and the citations therein. The accelerating bicycle has received scant attention, with [4] representing a noteworthy exception. In the context of the constant-speed straight-running bicycle small perturbations can be described by a pair of coupled second-order constant-coefficient ordinary differential equations in roll and steer [5]. The introduction of acceleration in these equations produces three influences; Firstly, it causes a force redistribution of the tire loading that can be computed using d’Alembert force ideas and the notion of an ‘effective wheel mass’ that recognises the moment required to accelerate the wheels’ spin inertia [19]. Secondly, acceleration introduces additional terms in each of the momentum balance equations given as (B1), (B2) and (B3) in [5]. And thirdly, acceleration-related terms appear in the (nonholonomic) tire-road contact constraint equations (B6) and (B7). In combination, these three influences produce a third acceleration-related stiffness matrix [4], [19]. Therefore, the extended model takes the form:

$$M\ddot{q} + vC\dot{q} + (gK_0 + aK_1 + v^2K_2)q = f, \quad (1)$$

in which v is the forward speed, $q = [\varphi \ \delta]^T$ and $f = [T_\varphi \ T_\delta]^T$. The bicycle’s roll and steer angles are given by φ and δ respectively. The moment T_φ is an externally applied roll moment and T_δ is the steering torque, which acts on the front frame and reacts on the rear frame. The constant 2×2 matrices M , C , K_0 and K_2 are defined in terms of the bicycle parameters [5]. The stiffness matrix K_1 introduces the effects of an acceleration a in the bicycle’s longitudinal direction. The

four entries of the K_1 matrix are

$$\begin{aligned} K_1(1,1) &= 0 \\ K_1(1,2) &= -\mu S_X + (I_{T_{xz}}/w + S_F) \cos(\lambda) \\ K_1(2,1) &= 0 \\ K_1(2,2) &= -\mu S_X \sin(\lambda) - m_A u_A \mu + ((\mu I_{T_{zz}} + I_{A\lambda z})/w \\ &\quad + S_F \mu (w + c - r_F \tan \lambda)/r_F - m_A u_A) \cos(\lambda), \end{aligned} \quad (2)$$

in which

$$S_X = m_B z_B + m_H z_H - r_R \left(m_R + \frac{I_{R_{yy}}}{r_R^2} \right) - r_F \left(m_F + \frac{I_{F_{yy}}}{r_F^2} \right). \quad (3)$$

The quantity S_X is used to calculate the acceleration-related front wheel normal load variation, which is given by $(aS_X)/w$. The notation and intermediate variables given in [5] have been adopted. For further details, a first-principles derivation of the K_1 matrix is given in Appendix A of [19]. Alternatively, one can refer to the analysis in [4] and adapt it to the present context. For the purpose of studying bursting-type instabilities, which occur on time scales over which acceleration-related vehicle speed variations are relatively unimportant, we will assume a constant machine speed. This situation is closely related to the analysis of the constant-speed machine on an inclined road surface [4], except that the longitudinal acceleration-related forces are aligned with the bicycle's main frame rather than with the inertial reference frame's x-axis [19]. In the case of the machine ascending or descending a hill, the machine yaw angle is a non-cyclic coordinate and yaw-angle-related terms appear in the equations of motion [4], [19]. If the acceleration-related inertial forces act in the direction of the line of intersection between the bicycle's rear wheel and the ground plane, the equations of motion become:

$$M\ddot{q} + vC\dot{q} + (gK_0 + a\bar{K}_1 + v^2K_2)q = f, \quad (4)$$

in which (2) is replaced with

$$\begin{aligned} \bar{K}_1(1,1) &= 0 \\ \bar{K}_1(1,2) &= -\mu S_X \\ \bar{K}_1(2,1) &= 0 \\ \bar{K}_1(2,2) &= -m_A u_A (\mu + \cos \lambda) - \mu S_X \sin \lambda. \end{aligned} \quad (5)$$

Since the machine is no longer accelerating, the real rather than effective wheel masses dictate the normal load variation on the front wheel and (3) is replaced with $S_X = m_T z_T$. Unlike (1), equation (4) is time-invariant. The frozen-time eigenvalues predicted by (1) are very similar to those predicted by (4) [19]. The acceleration-related linear model used here is more sophisticated than (4), but is based essentially on the same ideas. If the subject motorcycle is accelerating at $a \text{ m/s}^2$, then inertial forces of the form $\mathbf{F}_i = a\mathbf{m}_i$ are applied at the mass centres of each of the machine's six constituent masses in the corresponding longitudinal directions. Figure 4(a) shows constant-speed root loci for the subject motorcycle under straight-running and cornering conditions. As has been confirmed on the track, the subject motorcycle has no high-speed wobble and weave instabilities

under constant-speed conditions. The high-speed wobble-mode damping improves as the steady-state roll angle increases, with these increases accompanied by increases in the high-speed wobble-mode frequency. Increases in the roll angle have only a marginal effect on the high-speed weave-mode damping, which is accompanied by a reduction in the high-speed weave-mode frequency. The main purpose of Figure 4(a) is to provide a reference that shows the effect of the acceleration-related inertial forces that will now be introduced. Figure 4(b) illustrates the effect of accelerating

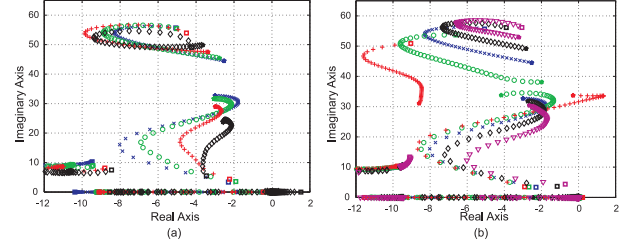


Fig. 4. (a) Root-loci for the subject motorcycle (with a steering damper fitted) under constant-speed conditions. Speed is the swept parameter for roll angles of 0° (blue \times), 15° (green \circ), 30° (red $+$) and 45° (black \diamond). The speed is varied from 9 m/s to 95 m/s in steps of 2 m/s. The highest speed is marked with a \star and the lowest speed with a \square . (b) Straight-running root-loci showing the wobble- and weave-mode eigenvalues of the subject motorcycle with the speed varied between 9 m/s and 95 m/s. A steering damper is fitted. The curves show the effect of acceleration-related inertial forces as follows: -4 m/s^2 (pink ∇), -2 m/s^2 (black \diamond), 0 m/s^2 (blue \times), 2 m/s^2 (green \circ) and 4 m/s^2 (red $+$). The highest speed is marked with a \star and the lowest speed with a \square .

and braking on the subject motorcycle's straight-running modal characteristics, and provides a first insight into the causes of the bursting found in Figures 1 and 3. Using the constant-speed plots as references, it is clear that braking causes the wobble-mode frequency to increase, while acceleration causes it to decrease. It is also evident that braking causes the weave-mode frequency to reduce, while acceleration causes it to increase. What is important in the context of the present research is the destabilizing interaction that occurs between the wobble and weave modes at higher speeds and under firm acceleration. This interaction causes the wobble-mode damping to increase substantially, while at the same time, the weave-mode damping reduces and even becomes unstable over the 60 m/s to 93 m/s speed ranges. These trends are counter to changes occurring under braking and lower levels of acceleration. The design challenge is to prevent these destabilizing interactions that occur under firm acceleration at elevated speeds. Figure 5 shows from a different perspective how acceleration produces a destabilizing interaction between the wobble and weave modes at high speed. Under braking, wobble frequency increases (relative to the constant speed case) by as much as 10 rad/s, while under acceleration it reduces by at least 10 rad/s in some cases. At 90 m/s the imaginary part of the wobble-mode eigenvalue varies from approximately 55 rad/s at -5 m/s^2 to approximately 32 rad/s at 5 m/s^2 . At the same time, the imaginary part of the weave mode reduces in frequency under braking, while it increases under acceleration. The resulting

destabilizing interaction is evident under firm acceleration over the 60 m/s to 90 m/s speed range. In contrast to the lower speeds illustrated, at 90 m/s the wobble-weave modal interaction causes the wobble (rather than the weave) mode to go unstable. Figure 6 shows the shape of the straight-

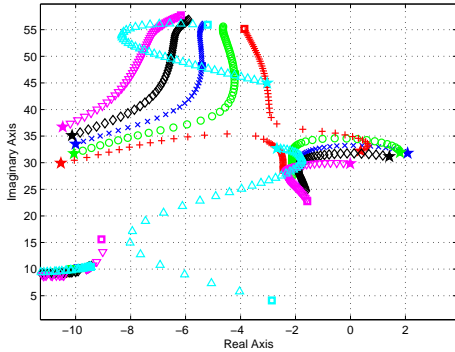


Fig. 5. Root-loci showing the effect of acceleration-related d'Alembert forces at five different speeds. The acceleration is swept over the interval $\pm 5 \text{ m/s}^2$; the highest acceleration is marked with a \star and the lowest acceleration with a \square . The subject motorcycle is fitted with a steering damper. The purple curve, annotated by ∇ , corresponds to a speed of 50 m/s. The black curve, \diamond , corresponds to a speed of 60 m/s. The blue curve, \times , corresponds to a speed of 70 m/s. The green curve, \circ , corresponds to a speed of 80 m/s. The red curve, $+$, corresponds to a speed of 90 m/s. The light blue curve, \triangle , is a reference plot corresponding to the zero-acceleration over the 10 m/s to 90 m/s speed range; the highest speed is marked with a \star and the lowest speed with a \square .

running weave mode eigenvector at 70 m/s and 80 m/s for a range of acceleration and braking forces. It is evident that firm acceleration causes a reduction in the relative magnitudes of the roll, yaw and lateral translation components of the weave-mode eigenvector, thereby making it more 'wobble-like'. Figure 7 shows the influence that acceleration and braking have on the root loci illustrated in Figure 4. These curves show that the straight-running influences of braking and acceleration extend to the cornering case in that braking tends to increase the wobble-mode frequency, while also degrading the damping of this mode. It can also be seen that braking reduces the weave-mode frequency, while also improving slightly the damping of this mode. The interaction between the wobble and weave modes, which occurs under firm acceleration at high speed, extends to the case of low roll angle cornering. As with straight running, the weave and wobble modes interact with the result that the wobble-mode damping increases significantly, while the weave-mode damping reducing to the point that the machine becomes unstable (at low roll angles). At 15° the machine will exhibit burst-type instabilities as it passes through the 80 m/s speed range. These predictions are aligned with Figures 1 and 3, and support the claim that constant-speed models can be used to predict acceleration-related bursting phenomena. Figure 8 investigates the bursting phenomenon from a frequency-response perspective using open-loop Nyquist diagrams for the steering damper loop in Figure 2 (a). The frequency responses correspond to the open-loop transfer function map-

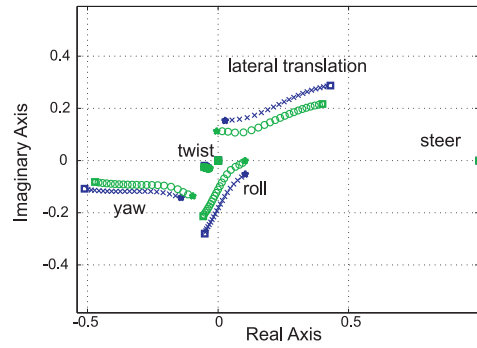


Fig. 6. Straight-running weave-mode eigenvector loci for the subject motorcycle (steering damper fitted) with acceleration-related inertial force the varied parameter for speeds of 70 m/s (blue \times) and 80 m/s (green \circ). The acceleration-related inertial forces are varied between -4 m/s^2 and 4 m/s^2 . The 13 eigenvector components corresponding to the generalised coordinates are shown; the eigenvectors are normalized so that the steer angle component is +1. The largest acceleration-related inertial force (4 m/s^2) is marked with a \star , while braking at -4 m/s^2 is marked with a \square . As with the classical weave mode, the five dominant components are: the machine's lateral translation, and the yaw, roll, frame twist and steer angles. The acceleration-related inertial forces reduce the amplitude of the lateral translation, and the yaw, roll and twist angle components. Under acceleration the weave mode of the subject motorcycle becomes 'wobble like'.

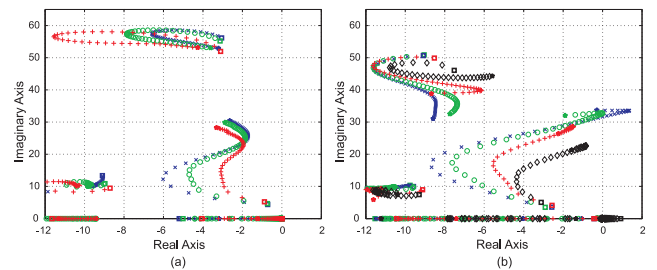


Fig. 7. Root-loci of the subject motorcycle with a steering damper fitted. Speed is the varied parameter for roll angles of 0° (blue \times), 15° (green \circ), 30° (red $+$) and 45° (black \diamond). The speed is varied from 9 m/s to 95 m/s in steps of 2 m/s. The highest speed is marked with a \star and the lowest speed with a \square . In (a) the braking-related acceleration is -4 m/s^2 , while in (b) the acceleration is 4 m/s^2 .

ping $t(s)$ to $s\delta(s)$ at 80 m/s with the damper gain included. Referring to (the red plot) in Figure 2 (b), two anticlockwise encirclements of the -1 point are required for closed-loop stability. Figure 8 shows that a damper will stabilize the machine at each illustrated value of acceleration and braking save for the 4 m/s^2 acceleration case when no damper will work, because there is no point on the negative real axis that is encircled twice. This leads to the conclusion that some form of phase compensation is required.

V. COMPENSATOR DESIGN

A. Performance Index

Following the approach taken in [1], a steering compensator will be synthesized using robust frequency domain optimization. The optimization of controllers for linear systems via \mathcal{H}_∞ frequency-response performance measures is now a well developed subject with most of the key ideas available in [17]. The optimization criterion is motivated by

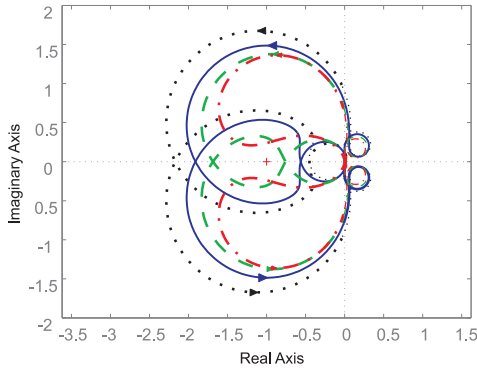


Fig. 8. Nyquist diagrams of the steering compensation loop for the straight-running subject motorcycle at 80 m/s. Four acceleration-related inertial forces are illustrated: -2 m/s^2 (black) dotted line, 0 m/s^2 (blue) solid line, 2 m/s^2 (green) dashed line and 4 m/s^2 (red) dash-dot line. Note that the machine is unstable at 80 m/s and 4 m/s^2 of acceleration for any value of steering damper.

a need for robust stability, as well as by the role played by road displacement forcing in triggering steer angle bursting phenomena. The objective is to minimize the worst-case closed-loop gain from road forcing disturbances to the steering angle for all operating conditions, while simultaneously ensuring that the open-loop Nyquist diagram encircles the -1 point the correct number of times (anticlockwise), while not getting ‘too close’ to it. For each frequency ω_i , the distance between the Nyquist diagram and the -1 point is given by $|1 - j\omega_i k(j\omega_i) p_{12}(j\omega_i)|$, which is the modulus of the classical sensitivity function [17]. The multi-objective \mathcal{H}_∞ index given in equation (6) will be used

$$J_f = \max_{\Omega} \left\{ \max \left\{ \max_{\omega_i} \left| \frac{p_{11}(j\omega_i)}{1 - j\omega_i k(j\omega_i) p_{12}(j\omega_i)} \right|, \max_{\omega_i} \left| \frac{\gamma}{1 - j\omega_i k(j\omega_i) p_{12}(j\omega_i)} \right| \right\} \right\}. \quad (6)$$

The first term in (6) is the closed-loop transfer function between road forcing disturbances and the steering angle, while the second is a fixed constant γ times the inverse of the distance of closest approach between the Nyquist diagram and the -1 point. The optimisation was carried out over a three-dimension set, Ω , of operating conditions. The set of linear models in Ω corresponded to: d’Alembert forces corresponding to accelerations of $-2, 0, 2 \text{ m/s}^2$; roll angles of $0, 3, 6, \dots, 48 \text{ deg}$, and speeds over the range 9 m/s to 95 m/s in steps of 2 m/s . The performance index (6) was evaluated over a 100-point frequency list with the points equi-spaced on a logarithmic scale that covers the range $10^{0.78}$ to $10^{1.85}$. This frequency range was selected to include all the maxima in the index (6). The weighting factor on the second term was set by trial to $\gamma = 16$.

B. Side Constraints

In order to define the optimization problem associated with (6) a number of side conditions must now be specified. Firstly, it is clear from Figure 8 that phase-lag compensation is required in the 4 m/s^2 acceleration case. For that reason the networks illustrated in Figure 9 will be studied, with

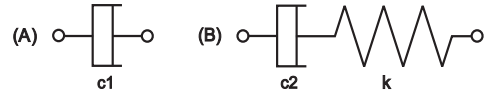


Fig. 9. Steering compensation networks. The conventional scheme is the pure damper shown in diagram (A), while the spring-damper lag compensator, which comprises a series-connected spring and damper combination is shown in diagram (B). The optimal damper value was found to be $c_1 = 8.06 \text{ Nms/rad}$, while the optimized spring-damper values are $k = 921.6 \text{ Nm/rad}$ and $c_2 = 7.30 \text{ Nms/rad}$.

the damper serving as a reference. Suppose the network admittance function $k(s)$, which is the controller in Figure 2 (a), maps the network terminal velocity $s\delta(s)$ into the corresponding torque $t(s)$. Then the admittance function for the damper-only network is $k(s) = c_1$, while that of the spring-damper network is $k(s) = k/(s + \frac{k}{c_2})$. In order to maintain network realizability, the component values are constrained to be positive. Secondly, a closed-loop stability constraint must be imposed. Recognizing that the low-frequency stability of the machine will be ensured by the rider, and not the compensation network, the stability constraint used here allows unstable low-frequency modes. This is achieved via the requirement that only closed-loop eigenvalues with an imaginary part greater than $0.45j$ must be confined to the left-half of the complex plane. No attempt is made to stabilize the marginally unstable capsized mode whose eigenvalue(s) is/are either real, or has/have a very small imaginary part. The optimization calculations make use of the MATLAB sequential quadratic programming algorithm `fmincon` [20].

VI. COMPENSATOR PERFORMANCE

Two optimization calculations were performed. The first was for the (A) configuration in Figure 9 and the second for the (B) configuration. The optimal damper value for the (A) configuration was found to be $c_1 = 8.06 \text{ Nms/rad}$, which is only slightly lower than that found on the subject motorcycle. When a series spring is included in the compensation network the optimal damper value reduces to $c_2 = 7.30 \text{ Nms/rad}$, while the optimal spring stiffness is $k = 921.6 \text{ Nm/rad}$. From these figures we conclude that the compensation network is simply a ‘slightly smaller damper in series with a stiff spring’, and so gross changes in behaviour are not to be expected. Figure 10 shows a Nyquist diagram of the compensated machine under high-speed straight-running conditions, where firm-acceleration-related bursting is the problem identified in Figure 8. As has already been shown, bursting under firm acceleration cannot be prevented using a steering damper alone, but it can be prevented using a spring-damper phase compensating lag network. The stabilizing influence of the network results from its ability to maintain two anticlockwise encirclements under firm acceleration conditions. The amplitude of the steering velocity burst is 1.835 rad/s when the optimized damper is installed (see Figure 3). This figure reduces to $1.58 \times 10^{-4} \text{ rad/s}$ when the optimized compensator is installed (with no other changes). Figure 11 illustrates the operation of the steering compensator under a range of high-speed straight-running braking and accelerat-

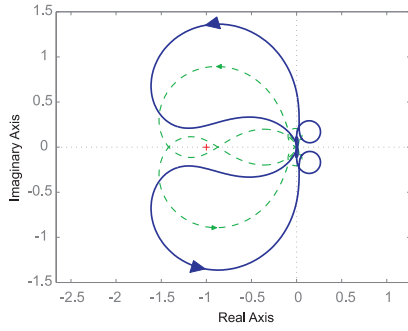


Fig. 10. Nyquist diagram for the cases when the machine is fitted with a steering damper (blue solid line), and the machine fitted with the steering compensator (green dashed line). The machine’s speed is 80 m/s, the roll angle is 0° and the acceleration-related inertial force is 4 m/s^2 . This diagram illustrates the improvement of the stability margins brought about by a steering compensator at high speed and high acceleration.

ing conditions. The influence of the lag compensator under firm acceleration is visible. In conventional terms, the closed-loop is operating with degraded stability margins, however concepts such as ‘stability’ and ‘stability margins’ should be used with care under short-period non-steady-state conditions such as those of interest here. Figure 12 shows the effect of

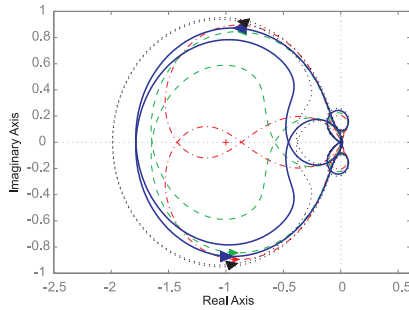


Fig. 11. Nyquist diagrams for the case of the subject motorcycle fitted with an optimized steering compensator. The acceleration-related inertial forces are: -2 m/s^2 (black) dotted line, 0 m/s^2 (blue) solid line, 2 m/s^2 (green) dashed line and 4 m/s^2 (red) dash-dot line. The machine speed is 80 m/s and its roll angle is 0° .

the steering compensator at low speed under moderate braking. When braking under straight-running, low-speed conditions the optimized damper has superior stability margins as compared with the optimized compensator. This observation motivates the need for braking-related models in the design optimization model set. If these models were not included, the resulting network would perform poorly under these conditions. Figure 13 is the steering compensated counterpart of Figure 4 (b). When the subject motorcycle is fitted with the steering compensator, rather than the optimized steering damper, the machine’s wobble mode frequency increases, which reduces the interaction between this mode and the weave mode. Indeed, at 4 m/s^2 , the compensator has succeeded in stabilizing the high-speed weave mode in the sense of the constant-speed model augmented with acceleration-related forces of inertia. Although the steering compensator has a destabilizing effect on the wobble mode under low-

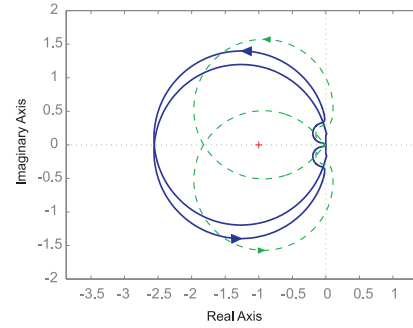


Fig. 12. Influence of a steering compensator at low speed and moderate braking. The Nyquist diagram for the case when the machine is fitted with the steering damper (blue) solid line and the compensator (green) dashed line. The machine’s speed is 30 m/s, the roll angle is 0° and the acceleration-related inertial force is -4 m/s^2 . This figure illustrates the detrimental influence of the steering compensator at low speeds and firm braking.

speed braking conditions, no further negative effects have been noticed. Figure 14 shows the effect of the steering

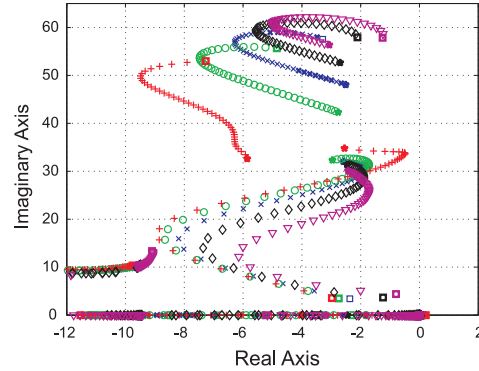


Fig. 13. Straight-running root-loci with speed the varied parameter for acceleration-related inertial force of -4 m/s^2 (pink ∇), -2 m/s^2 (black \diamond), 0 m/s^2 (blue \times), 2 m/s^2 (green \circ) and 4 m/s^2 (red $+$). The compensator is fitted. The speed is varied from 9 m/s to 95 m/s in steps of 2 m/s. The highest speed is marked with a $*$ and the lowest speed with a \square .

compensator under straight-running braking and accelerating conditions. It is clear from the (a) part of the figure that the steering compensator has no impact on the weave mode under braking conditions. It is also evident that the steering compensator tends to increase the wobble-mode frequency under braking conditions, while simultaneously reducing its damping. As is evident from the (b) part of the figure, that under firm acceleration, the steering compensator reduces the wobble-mode damping while simultaneously inhibiting high-speed weave-mode bursting.

VII. CONCLUSIONS

Burst oscillations arising in racing motorcycles at high speeds and under firm acceleration are investigated. The bursting phenomenon occurs at weave-mode frequencies under conditions that cause the classical wobble and weave modes to interact. Under race conditions this phenomenon can undermine rider confidence, and is consequently detrimental to lap times and potentially to rider safety. Curative

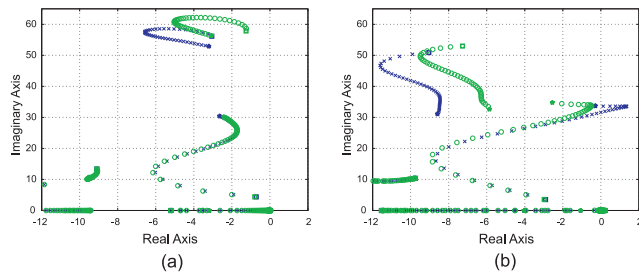


Fig. 14. Straight-running root-loci comparing the behaviour of the subject motorcycle fitted with a damper and a steering compensator. The speed is varied from 9 m/s to 95 m/s in steps of 2 m/s; the highest speed is marked with a \star and the lowest speed with a \square . The response corresponding to the damper-equipped machine is shown as the (blue) \times plot, while the compensator-equipped vehicle is shown as the (green) \circ plot. The (a) plot corresponds to -4 m/s^2 , while the (b) plot corresponds to 4 m/s^2 .

measures that make use of a simple mechanical steering compensator are proposed and tested on a high-fidelity simulation model. The proposed compensator introduces lag compensation into the steering-damper loop, and is constructed from a series combination of a conventional steering damper and a stiff spring. The mathematical model utilized here is a combination of conventional multibody mechanics, measurement-based suspension models, a high-fidelity chain drive representation and a modified Magic Formula based tire models. Unlike conventional Magic Formula based tire models, a ‘wide tire’ representation is used that allows the tire contact forces to move away from the wheels’ centre plane. As a result, elements of the tire moments are generated geometrically rather than by empirical formula. The steering dampers or more generally, steering compensators, are analysed in a robust control feedback system framework. There is novelty in the use of constant-speed models, in combination with d’Alembert-type inertial forces to study the machine dynamics under braking and accelerating conditions. This approach is justified by multiple time scales ideas. The strong advantage gained from this approach is the ability to study an inherently time-varying problem in a time-invariant framework, which facilitates the use of classical frequency response and robust control ideas. The motorcycle studied here has wobble- and weave-mode frequencies that are separated by approximately 1.6 Hz at high constant speed. When the machine accelerates at high speed this frequency separation disappears and the wobble and weave modes interact thereby producing an unstable weave-like mode that produces bursting oscillations. When the machine speed reduces under braking, the wobble and weave mode frequencies separate and no modal interaction occurs. Nyquist diagrams show that the modal interaction phenomenon results from a lack of phase compensation in the steering damper loop, and that once this is introduced, the bursting phenomena are strongly attenuated to a level that is no longer noticeable. The machine’s tolerance to lag compensation in the steering loop is restricted by the fact that excessive lag compensation leads to poor handling under braking at low speeds. A good compromise has been struck

by the parameter optimization. The general issue of the practical implementation of passive mechanical compensators is the subject of continuing investigation. This includes the fabrication of general integrated mechanical networks. Due to the extreme simplicity of the network required here, the current fabrication problem is easily solved. Other steering compensation problems may be more challenging.

REFERENCES

- [1] S. Evangelou, D. J. N. Limebeer, R. S. Sharp, and M. C. Smith, “Steering compensators for high-performance motorcycles,” *ASME J. Applied Mechanics*, vol. 74, no. 5, pp. 332–346, 2007.
- [2] R. S. Sharp and C. J. Alstead, “The influence of structural flexibilities on the straight running stability of motorcycles,” *Vehicle System Dynamics*, vol. 9, no. 6, pp. 327–357, 1980.
- [3] P. T. J. Spierings, “The effects of lateral front fork flexibility on the vibrational modes of straight-running single-track vehicles,” *Vehicle System Dynamics*, vol. 10, no. 1, pp. 21–35, 1981.
- [4] J. P. Meijaard and A. L. Schwab, “Linearized equations for an extended bicycle model,” in *III European Conference on Computational Mechanics, Structures and Coupled Problems in Engineering* (C. A. Mota Soares et al., ed.), (Lisbon, Portugal), pp. 1–18, 5-9 June 2006.
- [5] J. P. Meijaard, J. M. Papadopoulos, A. Ruina, and A. L. Schwab, “Linearized dynamics equations for the balance and steer of a bicycle: a benchmark and review,” *Proceedings Royal Society A*, vol. 463, pp. 1955–1982, 2007.
- [6] R. S. Sharp, “The stability of motorcycles in acceleration and deceleration,” in *Inst. Mech. Eng. Conference Proceedings on Braking of Road Vehicles*, (London), pp. 45–50, MEP, 1976.
- [7] D. J. N. Limebeer, R. S. Sharp, and S. Evangelou, “The stability of motorcycles under acceleration and braking,” *Jour. Mech. Eng. Sci.*, vol. 215, no. 9, pp. 1095–1109, 2001.
- [8] S. Evangelou and D. J. N. Limebeer, “Lisp programming of the ‘sharp 1971’ motorcycle model.” Unpublished report, <http://www3.imperial.ac.uk/controlandpower/research/motorcycles/reports>, 2000.
- [9] S. Evangelou and D. J. N. Limebeer, “Lisp programming of the ‘sharp 1994’ motorcycle model.” Unpublished report, <http://www3.imperial.ac.uk/controlandpower/research/motorcycles/reports>, 2000.
- [10] R. S. Sharp, S. Evangelou, and D. J. N. Limebeer, “Improved modelling of motorcycle dynamics,” in *ECCOMAS Thematic Conference on Advances in Computational Multibody Dynamics* (J. Ambrósio, ed.), (Lisbon), July 1–4 2003. MB2003-029 (CD-ROM).
- [11] R. S. Sharp and D. J. N. Limebeer, “A motorcycle model for stability and control analysis,” *Multibody System Dynamics*, vol. 6, no. 2, pp. 123–142, 2001.
- [12] R. S. Sharp, S. Evangelou, and D. J. N. Limebeer, “Advances in the modelling of motorcycle dynamics,” *Multibody System Dynamics*, vol. 12, no. 3, pp. 251–283, 2004.
- [13] R. S. Sharp, S. Evangelou, and D. J. N. Limebeer, “Multibody aspects of motorcycle modelling with special reference to Autosim,” in *Advances in Computational Multibody Systems* (J. G. Ambrsio, ed.), pp. 45–68, Springer-Verlag, Dordrecht, The Netherlands, 2005.
- [14] H. B. Pacejka, *Tyre and Vehicle Dynamics*. Oxford: Butterworth Heinemann, 2002. ISBN 0-7506-5141-5.
- [15] Anon., *Adams/tire r2 help*, 2005.
- [16] S. A. Evangelou, D. J. N. Limebeer, and M. Tomas-Rodriguez, “Suppression of burst oscillations in racing motorcycles,” *Transactions of the ASME, Journal of Applied Mechanics*, In Reviewing, 2010.
- [17] M. Green and D. J. N. Limebeer, *Linear Robust Control*. Englewood Cliffs, New Jersey 07632: Prentice Hall, 1995.
- [18] D. Limebeer and R. Sharp, “Bicycles, motorcycles and models,” *IEEE Control Systems Magazine*, vol. 26, no. 5, pp. 34–61, 2006.
- [19] D. J. N. Limebeer and A. Sharma, “Burst oscillations in the accelerating bicycle,” *To appear in ASME Journal of Applied Mechanics*, pp. 1–31, 2010.
- [20] The Mathworks Inc., *MATLAB 6 Reference Manual*, 2000.